AD NUMBER

ADA177273

LIMITATION CHANGES

TO:

Approved for public release; distribution is unlimited.

FROM:

**Distribution authorized to U.S. Gov't. agencies and their contractors;
Administrative/Operational Use; 1986. Other requests shall be referred to Office of Naval Research, 875 Randolph Street, Arlington, VA 22203-1995.**

AUTHORITY

ONR ltr, 9 Feb 1987

SM Report 86-8

MEASUREMENT OF THE J INTEGRAL WITH CAUSTICS: AN EXPERIMENTAL AND NUMERICAL INVESTIGATION

by

Alan T. Zehnder*, Ares J. Rosakis, and R. Narasimhan***

Graduate Aeronautical Laboratories
California Institute of Technology
Pasadena, CA 91125

1986 (?)

* Graduate Research Assistant.

** Assistant Professor of Aeronautics and Applied Mechanics.

ABSTRACT

The optical method of caustics as applied to the measurement of the J integral in plastically deforming materials was studied numerically and experimentally. The numerical calculations modeled a cracked body loaded under Mode I, plane stress, small scale yielding conditions. The results were used to generate simulated optical patterns for caustics obtained from both inside and outside the crack tip plastic zone. These caustics were compared with corresponding caustics observed experimentally. In addition, the region of dominance of the plane stress, HRR field was investigated, and the effect of plasticity on the accuracy of caustics from the elastic region outside the plastic zone was determined. The extent of the region of three dimensionality near the crack tip and its effect on the method of caustics was also investigated.

Keywords:

J integral, elastic-plastic fracture, HRR field, caustics, finite elements

1. INTRODUCTION

In recent years the optical method of caustics has been developed into a very successful experimental tool for studying linear elastic fracture mechanics problems. In such problems, the method of caustics can be used for the direct measurement of the stress intensity factor, K_I [1,2]. Particularly important applications of caustics have been made in dynamic fracture mechanics where the stress intensity factor cannot generally be determined analytically. The past success of caustics has led to efforts to extend the method to applications in elastic plastic fracture.

Some preliminary work [3,4], based on the assumption of the validity of the plane stress, HRR, asymptotic crack tip field [5,6], demonstrated that the value of the J integral can be directly measured with caustics. Unfortunately the region of dominance of the plane stress HRR field has not been accurately established. Thus the conditions under which the analytical results reported in [3,4] are valid are uncertain. Experimental results given in [4,7,8] indicate that the method is promising and is worthy of further investigation.

In this paper the method of caustics is investigated experimentally and numerically. One of the goals of this work is to provide an analysis of caustics which is based on a full field, small scale yielding, finite element solution. In small scale yielding, well outside the plastic zone, the elastic, singular stress field dominates. Inside the plastic zone, very near the crack tip, the HRR field dominates. In the transition region between these two fields no analytical solution is known. Thus no analysis of the method of caustics exists for this region. This places certain limitations on the applicability of caustics. To quantify the limitations, the extent of dominance of the plane stress HRR field is studied numerically. In addition, an analysis of caustics based on the numerical results is introduced. This analysis is not limited by the assumption of a particular asymptotic field.

For caustics obtained from the elastic region surrounding the crack tip plastic zone, an analysis based on the linear elastic K_I field may be used. However crack tip plasticity often affects caustics, causing errors in the measurement of K_I. The resulting errors are investigated here experimentally.

The analysis of the method of caustics applies to cracked, planar bodies that are thin enough so that the state of deformation is one of plane stress. However, there is a region near the crack tip where the deformation fields are three dimensional. Experiments were performed to investigate the extent of the region of three dimensional fields for plastically deforming materials, and to determine the effect of three dimensionality on the accuracy of the method of caustics as based on plane stress fields.

2. THE METHOD OF CAUSTICS

Consider a set of parallel light rays normally incident on a planar, reflective specimen. The specimen surface was initially optically flat but it is deformed due to the tensile crack tip loading. The deformed shape of the specimen surface is such that the virtual extension of the reflected light rays forms an envelope in space as illustrated in Fig. 1. This surface, called the "caustic surface" is the locus of points of maximum luminosity. Its intersection with a plane located a distance z_o behind the specimen is called the "caustic curve". This curve bounds a dark region, called the "shadow spot". By placing a camera in front of the specimen to collect the reflected light rays and by focusing the camera behind the

specimen the caustic can be photographed.

Suppose that light reflected from a point (x_1,x_2) on the specimen intersects the plane at z_o at a point (X_1,X_2), where (x_1,x_2) is a coordinate system on the specimen centered on the crack tip and (X_1,X_2) is a system translated by a distance z_0 behind the specimen. Then (X_1,X_2) are given by the mapping [1]

$$X_\alpha = x_\alpha - 2z_o \frac{\partial f(x_1,x_2)}{\partial x_\alpha} \qquad \alpha = 1,2, \tag{1}$$

where $f(x_1,x_2) = -u_3(x_1,x_2)$, the out of plane surface displacement of the specimen. As discussed in [9] a caustic curve will exist if and only if the Jacobian determinant of the mapping vanishes,

$$J(x_1,x_2,z_o) = \det\left[\frac{\partial X_\alpha}{\partial x_\beta}\right] = 0. \tag{2}$$

The locus of points on the specimen satisfying J = 0 is called the "initial curve". All points on the initial curve map onto the caustic curve. In addition all points inside and outside the initial curve map outside the caustic. Since the light that forms the caustic curve is reflected from the initial curve, whatever information is conveyed by the caustic comes from this curve only. Equation (2), defining the initial curve depends on z_o. Thus by varying z_o the initial curve position may be varied. If z_o is large then the initial curve will be located far away from the crack tip. If z_o is small then the initial curve will be close to the crack tip.

When the initial curve is well outside the crack tip plastic zone the analysis of caustics based on the linear elastic K_I field may be used. In such cases the Mode-I, plane stress, out of plane displacement field is given by

$$u_3 = \frac{-\nu h K_I}{E\sqrt{2\pi r}} \cos\frac{\theta}{2}, \tag{3}$$

where E is the elastic modulus, ν is Poisson's ratio, h is the specimen thickness, and r and θ are polar coordinates. By substituting Eq (3) into Eqs (1) and (2) it is found that the caustic

is an epicycloid and that K_I is related to the caustic diameter D (width of the caustic in the X_2 direction) by [1,2]

$$K_I = \frac{ED^{5/2}}{10.7 z_o \nu h}. \tag{4}$$

The initial curve is circular and its radius r_o is

$$r_o = 0.316D = \left[\frac{3h\nu K_I z_o}{2\sqrt{2\pi}E}\right]^{2/5}. \tag{5}$$

When the initial curve is within the region of dominance of the plane stress HRR field an alternate analysis of caustics must be used. For a material with a stress strain curve that may be described by the Ramberg-Osgood model

$$\frac{\epsilon}{\epsilon_o} = \frac{\sigma}{\sigma_o} + \alpha\left(\frac{\sigma}{\sigma_o}\right)^n,$$

where σ_o and ϵ_o are the yield stress and yield strain in tension, the asymptotic, out of plane displacement is given by [5,6]

$$u_3 = \frac{\alpha\sigma_o h}{2E}\left[\frac{JE}{\alpha\sigma_o^2 I_n r}\right]^{\frac{n}{n+1}}\left[E_{rr}(\theta,n) + E_{\theta\theta}(\theta,n)\right] \tag{6}$$

where I_n is a numerical factor that depends on the hardening exponent n and E_{rr} and $E_{\theta\theta}$ are dimensionless functions of θ and n. Substitution of Eq (6) into Eqs (1) and (2) yields [3]

$$J = S_n \frac{\alpha\sigma_o^2}{E}\left[\frac{E}{\alpha\sigma_o z_o h}\right]^{\frac{n+1}{n}} D^{\frac{3n+2}{n}}, \tag{7}$$

where S_n is a numerical factor dependent on n. For a non-hardening material [4]

$$J = \frac{\sigma_o D^3}{13.5 z_o h}. \tag{8}$$

The caustic for a hardening exponent of n=9 is shown in Fig. 2. Figure 2a shows the predicted caustic and Fig. 2b shows the caustic observed in an experiment. The plastic zone can be seen surrounding the caustic of Fig. 2b demonstrating that the caustic came from light reflected from within the plastic zone.

Unlike the elastic case the initial curve, sketched in Fig. 3, is no longer circular; it depends on the hardening level of the material. The point on the initial curve that maps to the maximum value of X_2 on the caustic curve is located at an angle θ_{max} from the x_1 axis. Let the distance to this point from the crack tip be called r_o, the initial curve size. It is important to know the location of this point since it is mapped to the maximum diameter of the caustic, which is used in the interpretation of the results. It was shown in [8] that θ_{max} varies from 72° to 56° as n varies from 1 to ∞. For a power law hardening material [8]

$$r_o = \begin{cases} 0.385D & n=9 \\ 0.40D & n=50 \end{cases}. \tag{9}$$

Note that Eqs (3)-(9) are based on the assumption of the validity of particular asymptotic fields. In the next section an attempt is made to eliminate this restriction by constructing caustics based on a full field numerical solution.

3. NUMERICAL ANALYSIS

3.1. Formulation.

The numerical calculations modeled a semi-infinite crack under Mode-I, plane stress, small scale yielding conditions. The displacements from the singular, elastic crack tip field

$$u_\alpha(r,\theta) = K_I \sqrt{\frac{r}{2\pi}}\ \hat{u}_\alpha(\theta)$$

were specified on a circle of radius of approximately 3400 times the the smallest element length, as shown in Fig. 4. The maximum extent of the plastic zone was contained within 1/30 of this radius. The cutout in Fig. 4a is a fine mesh region around the crack tip which is shown in detail in Fig. 4b. An incremental J_2 plasticity theory was used. The material obeyed the von Mises yield criterion and followed a piecewise power hardening law in uniaxial tension of the form

$$\frac{\epsilon}{\epsilon_o} = \begin{cases} \dfrac{\sigma}{\sigma_o} & \sigma \le \sigma_o \\ \left(\dfrac{\sigma}{\sigma_o}\right)^n & \sigma > \sigma_o \end{cases}$$

with hardening exponent n=9. This value was chosen to match the 4340 steel used in the experiments. All plasticity was confined to the active region (Fig. 4a) consisting of 1704 four-noded isoparametric quadrilaterals. The quadrilaterals were formed from 4 constant strain triangles with static condensation of the internal node. Static condensation was used in the region around the active mesh that always remained elastic. The stress computations were performed using a tangential stiffness-radial return method with subincrementation [10]. The nonlinear finite element equilibrium equations were solved incrementally using the iterative Newton-Raphson method [11].

After the element nearest to the crack tip has yielded, the load, applied through the stress intensity factor K_I, was increased in steps of 5-10% of the value at yield until the extent of the plastic zone ahead of the crack tip was 50 times the smallest element size.

3.2. Results.

The calculated and experimentally observed plane stress, crack tip plastic zones are shown in Fig. 5. A point was plotted for every element that had yielded, thus defining the calculated plastic zone in Fig. 5a. Figure 5b shows visual evidence of plastic deformation observed on the surface of a thin, compact tension specimen of 4340 steel with a hardening exponent of n=8.7. It is seen that the calculated and observed plastic zones agree in shape. Both calculations and experiment show that the extent of the plastic zone ahead of the crack tip is $r_p=0.25(K_I/\sigma_o)^2$.

The stress distribution σ_{22}/τ_o ahead of the crack is shown in Fig. 6. The non-dimensionalization of x_1 by $(K_I/\sigma_o)^2$ is used because the plastic zone scales with this parameter. The computed stress agrees with the stresses of the plane stress HRR field to within 1% when $x_1 \leq 0.08(K_I/\sigma_o)^2$, i.e. $x_1<0.3r_p$. In Fig. 7 the plastic strain distributions $\epsilon^p_{22}/\epsilon_o$ and $\epsilon^p_{33}/\epsilon_o$ are compared to the strains predicted by the HRR solution. Again it is seen that the numerical results agree with the HRR feld up to $x_1 \sim 0.3r_p$. Of particular interest is the result for $\epsilon^p_{33}/\epsilon_o$ since this is related to the out of plane displacement, which is important to the method of caustics.

The stresses ahead of the crack are compared to the linear elastic K_I field in Fig. 8. At the boundary of the plastic zone ($x_1=0.25(K_I/\sigma_o)^2$) σ_{22} begins to decrease rapidly, making a transition to the linear elastic solution as x_1 increases. It is seen that the linear elastic field agrees with the actual stress field when $x_1 \geq 1.5\ r_p$.

3.3. Numerically Generated Caustics.

To provide a means to analyze caustics that is not dependent on the assumption of dominance of the HRR or K_I fields, caustics were generated using the results of the FEM analysis. The out of plane surface displacements, shown here in Fig. 9, were smoothed using a least squares scheme [12] and caustics were generated by mapping light rays point by point using Eq (1) for different values of z_o. The caustics are shown in Fig. 10 for values of r_o/r_p from 0.19 to 1.3. It is seen that for $r_o/r_p=0.19$ the numerically simulated caustic agrees in shape with the caustic predicted using the the HRR field, Fig. 2. When $r_o/r_p=1.3$ the numerically simulated caustic, Fig. 10f, agrees with the caustic predicted using the elastic, K_I field. In the region between $r_o/r_p=.19$ and 1.3 there is a transition

from the "HRR like" caustic to the "elastic caustic". It is seen that for r_o/r_p as small as 0.30 (Fig. 10b) the caustic shape deviates from the HRR shape.

The numerical caustics were produced for a fixed level of applied K_I, or J since $J=K_I^2/E$. By measuring the caustics a relationship between the caustic diameter and the known value of J was determined for all values of r_o/r_p. The relationship is given in Fig. 11 where the non-dimensionalized caustic diameter is plotted as a function of the non-dimensionalized J integral. The bars on the numerical results indicate the uncertainty in D due to the discretization of the finite elements. The solid line gives the relationship for caustics from the K_I dominant region, Eq (4) with ν= 0.3. The dashed line gives the relationship for caustics from the HRR dominant region, Eq (7), with α=1.0. The value of α=1.0 was chosen to match the material idealization of the numerical model. Note, however, that Eq (7), is a very weak function of α.

For large values of z_0 (large initial curves) the numerical results approach the elastic relation, Eq (5). For small values of z_0 (initial curve close to the crack tip) the numerical results agree with the relation obtained on the basis of the HRR field, Eq (7).

4. DESCRIPTION OF EXPERIMENTS

To experimentally determine the range of validity of the caustics measurements, the J integral (J_{caus}) or the stress intensity factor (K_{caus}) was measured with caustics using different initial curves. These quantities were simultaneously measured from the boundary conditions and are denoted by J_{BC} and K_{BC}. The values were then compared for different conditions.

The caustics were photographed using the apparatus illustrated in Fig. 12. The system consisting of the lens and screen forms a telephoto camera that is focused on a virtual image plane at a distance z_o behind the specimen. Light reflected from the specimen forms a caustic on the screen which is then photographed with a 35 mm camera. Graph paper on the screen allows the magnification from the screen to the film to be determined and the thin lens equation is used to calculate the magnification from the virtual image plane to the screen. By varying the distance from the lens to the screen and by using different focal length lenses, the system can be focused at different distances z_o behind

the specimen. Varying z_o varies the initial curve, allowing data to be obtained from different distances from the crack tip.

Note that to have large z_o one must make the distance from the lens to the screen small. In order to maintain a good magnification, a long focal length lens should be used when z_o is large.

The initial curve was calculated from the caustic diameter using Eq (5) for $r_o > r_p$ and Eq (9) for $r_o < r_p$. In transition regions where neither the HRR or the elastic field dominates, or in three-dimensional regions, these equations are approximate. However, r_o should always be bounded by the two values, 0.316D and 0.40D, (Eqs (5) and (9)) and thus any calculated value of r_o using these equations is approximately correct even in the transition regions.

For these tests, loading beyond relatively small scale yielding conditions was not applied. Thus only the applied load needed to be measured to determine J. Values of K_{BC} (and hence J_{BC}) were calculated using formulas given in [13] of the form

$$K_I = f\,(P, a', geometry) \tag{10}$$

where P is the load applied to the specimen. A correction to the crack length to account for the plastic zone in calculating K_I was used. The correction, discussed in [14] is given by

$$a' = a + \phi r_y$$

where a is the crack length,

$$r_y = \frac{1}{2\pi}\,\frac{n-1}{n+1}\,\left(\frac{K_I}{\sigma_o}\right)^2$$

and

$$\phi = \frac{1}{[1-(P/P_{LIM})^2]}.$$

Equations for the limit load, P_{LIM}, are given in [14].

The specimen dimensions and geometries are given in Fig. 13. The test specimens were lapped optically flat and polished to a mirror finish. The pre-crack was cut with a wire electric discharge machine, producing a crack tip diameter of 0.3 mm. Annealed 4340 steel and cold-rolled 1018 steel were used. The heat treatment of the 4340 steel was: $675°C$ for 1.5 hours, oil quench, then anneal at $520°C$ for 1 hour and air cool. The material properties were: yield stress $\sigma_o = 830\ MPa$, hardening exponent n=8.7, and $\alpha = 3.3$ for a best fit of the uniaxial tension properties to the Ramberg-Osgood material model. The 1018 steel was used as received. It had $\sigma_o = 560\ MPa$ with no hardening.

The tests proceeded by loading the specimen to some level and then maintaining that level while caustics were photographed for different values of z_o. The load was then increased a step and the process repeated.

5. EXPERIMENTAL RESULTS AND DISCUSSION

5.1. Sequence of Caustics.

A sequence of photographs of caustics is shown in Fig. 14. These photographs are from specimen 28, loaded such that $r_p \approx 3.4mm$. Only the distance z_0 was varied, thus varying the initial curve size r_0. The parameter r_0/r_p in the figure is the ratio of the initial curve size to plastic zone size. The plastic zone size r_p was estimated by measuring the extent of the visual evidence of plastic deformation seen in the photographs. The initial curve size r_0 was estimated using Eq (9) when $r_0/r_p<1$ and Eq (5) when $r_0/r_p>1$. It is seen from Fig. 14 that for $r_0/r_p \leq 0.35$ the caustics agree in shape with the caustic predicted from the plane stress HRR field (Fig. 2a). For $r_0/r_p=1.4$ (Fig. 14f) the caustic has the shape predicted using the singular elastic field.

Comparing the experimentally observed caustics with the numerically generated ones of Fig. 10 it is seen that in both cases there is a transition from an "HRR caustic" to an "elastic caustic" as r_0/r_p goes from 0.19 to 1.4. The transition away from the HRR caustic occurs at $r_0/r_p \approx 0.35$ for the experimental results and at $r_0/r_p \approx 0.30$ for the numerical results. Thus it appears that the transition from the HRR caustic to the elastic caustic occurs sooner in the

numerical model than in the experiments. However, the general trend is similar in each case.

By comparing the shapes of the experimentally observed caustics to the predicted caustic shape (Fig. 2a) further information on the region of dominance of the HRR field can be obtained. If the caustic is not shaped similar to the predicted caustic then the displacement fields near the initial curve cannot correspond to that of the HRR field. The caustics of Fig. 14 deviate from the predicted shape for $r_0/r_p \geq 0.35$ indicating that under small scale yielding an upper bound for the dominance of the HRR field is $r \approx 0.35 r_p$.

5.2. Effect of Plasticity on Elastic Caustics.

Under conditions of plane stress, small scale yielding the elastic singular field dominates at some distance outside the plastic zone. Thus when the initial curve radius r_0 satisfies $r_0 \gg r_p$ and $r_0 \ll a$ where a is the crack length or some other relevant in plane specimen dimension, K_I may be measured with caustics by applying Eq (4).

The results shown in Fig. 8, show that the elastic singular field does not agree with the actual stress field when $r < 1.5 r_p$. Thus values of K_I measured with caustics are expected to be affected by the plastic zone when $r_0 < 1.5 r_p$.

To quantify the effect of plasticity on caustics from outside the plastic zone, experiments were performed measuring K_I from caustics, K_{caus}, at different distances from the crack tip and comparing K_{caus} to K_I measured from the boundary conditions, K_{BC}.

The results are presented in Fig. 15 where K_{caus}/K_{BC} is plotted vs. r_0/r_p. The initial curve radius r_0 is calculated using Eq (5). For all of the tests r_p was calculated using the numerical results

$$r_p = 0.25 \left(\frac{K_I}{\sigma_0} \right)^2 \tag{11}$$

for the 4340 steel (n=8.7) and using the estimation

$$r_p = \frac{1}{\pi}\left(\frac{K_I}{\sigma_0}\right)^2 \tag{12}$$

for the 1018 steel ($n\rightarrow\infty$).

According to [15], for elastic solids plane stress conditions prevail for $r>0.5h$, where h is the specimen thickness. Therefore only caustics satisfying $r_0>0.5h$ were plotted, ensuring plane stress conditions. The parameter r_p/w in the figure is the ratio of plastic zone size to uncracked ligament size, w. This parameter indicates the extent of yielding that has occured. No data were obtained for $r_p/w>.046$ because beyond that level of yielding it was not possible to observe a caustic that was shaped like the predicted caustic since small scale yielding conditions were no longer satisfied. Some data points are given for $0.7<r_0/r_p<1.0$. It was observed that for r_0/r_p as small as 0.7 the caustic curve remained close to the elastic shape. Thus it is appropriate to present data for $r_0/r_p\approx 0.7$ along with data for $r_0>r_p$.

The results of Fig. 15 show that away from the plastic zone Eq (4) is valid. However, for $r_0\leq 1.5r_p$, K_{caus}/K_{BC} deviates from 1.0 indicating that serious errors will occur if Eq (4) is applied for the evaluation of caustics in this range. This limit does not appear to depend on hardening for $n\geq 9$ since the 4340 steel and the 1018 steel data are consistent with each other.

As stated above the caustics retain the shape predicted by the elastic analysis even for r_0/r_p as small as 1.0. Thus the effect of the plastic zone on the caustic cannot be judged by observation of the caustic shape. The invarience of the shape of the caustic is explained by the numerical results. In Fig. 16 the angular distribution of the sum $\sigma_{11}+\sigma_{22}$ is given for different distances from the crack tip. It is seen that $\sigma_{11}+\sigma_{22}$ generally follows the singular elastic field even for r_0/r_p as small as 1.2. This result is important because it is the out of plane displacement $u_3 = -\frac{h\nu}{2E}\left(\sigma_{11}+\sigma_{22}\right)$ that is relevant to caustics, and because the shape of the caustics is mainly determined by the angular distribution of u_3. Since the angular distribution of u_3 is in good agreement with the singular elastic field, the caustic shapes do not deviate much from the predicted shape as $r_0\rightarrow r_p$. It is interesting to note that for small values of r_0/r_p the angular variation of individual stress components

σ_{11},σ_{22} does not follow the elastic K_I field distribution as well as the sum $\sigma_{11}+\sigma_{22}$ does.

5.3. Three Dimensional Effects.

It has been demonstrated above that the plane stress, HRR field dominates for $r \leq 0.30 r_p$. Thus the application of Eq. 7 for analyzing caustics is restricted to $r_0/r_p < 0.30$ if plane stress conditions are satisfied. However, due to the finite thickness of an actual test specimen there is a region near the crack tip in which the deformation field is three dimensional. It was shown in [15] that for elastic materials this region extends for distances from the crack less than one half of the specimen thickness. Here the three dimensional effects in elastic-plastic materials are investigated.

Experiments were performed measuring J_{caus} using caustics at different distances from the crack tip and then comparing J_{caus} to J_{BC}, measured from the boundary conditions. The specimens used for these tests are the same specimens that were used for investigating the caustics from outside the plastic zone. The only difference is that here the initial curve was placed well inside the plastic zone, and the plastic zone size was generally larger.

The collective results are presented in Fig. 17 where J_{caus}/J_{BC} is plotted vs. r_0/h. The initial curve size, r_0, was calculated using Eq (9). Only data points corresponding to caustics for which the aspect ratio D_y/D_x was in good agreement with the value predicted by the HRR field were plotted. Here D_y and D_x are the sizes of the caustic in the x_2 and x_1 directions. This was done to insure that only the three dimensional effects were being investigated. Other effects, such as the variation of caustic shape as r_0/r_p increases, are thus minimized. The maximum ratio of initial curve to plastic zone size was $r_0/r_p \leq 0.45$.

No results are given in Fig. 17 for $r_0/h > 0.6$. The reason for this is that in a given test (h, r_p constant),as r_0/h is increased, r_0/r_p is also increased. When r_0/r_p becomes large the caustic shape is no longer similar to the HRR shape and thus a calculation of J using the analysis of caustics based on the HRR field is meaningless in such cases. It was found that r_p could not be increased indefinitely for two reasons. First, the thin specimens used here are prone to out of plane bending and buckling at the high loads needed to make r_p large. Second, extensive plastic deformation reduces the reflectivity of the specimens reducing the definition of the resulting caustic.

The results show that for $r_0/h \leq 0.6$, J_{caus}/J_{BC} is less than one, indicating that three dimensional effects are important in that region. The extent of the region of three dimensionality seems to be larger than the extent for elastic materials. The plane stress crack tip solution, Eq (3) predicts that $u_3 \rightarrow \infty$ as $r \rightarrow 0$. However, since this is impossible, the actual u_3 is less than predicted. Thus so are the values of J_{caus}/J_{BC} since the size of the caustic increases with increasing u_3 and $\partial u_3/\partial x_\alpha$.

The results do not seem to depend on specimen configuration or on the particular steel. The reason for this consistency is that the tests were all carried out under nominally small scale yielding conditions, thus the only in plane distance that is important is the plastic zone size. Also note that the 4340 steel has a relatively low hardening making it nearly elastic-perfectly plastic like the 1018 steel.

6. CONCLUSIONS

Application of the method of caustics for the measurement of the J integral in plastically deforming materials was investigated. It was found that under small scale yielding conditions the plane stress, HRR field dominates for $r<0.3r_p$. Thus the application of caustics as based on the HRR field is restricted to initial curves satisfying $r_0<0.3r_p$. For caustics obtained from the elastic region the presence of a plastic zone introduces errors in the measurement of the elastic stress intensity factor when $r_0<1.5r_p$. An analysis of caustics, based on the results of the plane stress, full field numerical solution, was introduced. This analysis is valid for all initial curves. In an actual test specimen there is a region near the crack tip where the deformation field is not one of plane stress but is three dimensional. It was found that the extent of this region for plastically deforming materials extends to at least $r<0.6h$, where h is the specimen thickness.

7. ACKNOWLEDGEMENTS

The support of the Office of Naval Research through contract N00014-85-K-0596 and of the National Science Foundation through contract MEA-83-07785 is gratefully acknowledged.

8. REFERENCES

1. Manogg, P., "Anwendung der Schattenoptik zur Untersuchung des Zerreissvorgangs von Platten," Dissertation, Freiburg, West Germany, 1964.
2. Beinert, J. and Kalthoff, J.F., in *Mechanics of Fracture*, Vol. VII, G. Sih ed., Sijthoff and Noordhoff, 1981, pp. 281-330.
3. Rosakis, A.J., Ma, C.C., and Freund, L.B., *Journal of Applied Mechanics*, Vol. 105, 1983, pp. 777-782.
4. Rosakis, A.J., and Freund, L.B., *Journal of Engineering Materials and Technology*, Vol. 104, 1982, pp. 115-120.
5. Hutchinson, J.W. *Journal of the Mechanics and Physics of Solids*, Vol. 16, 1968, pp. 13-31.
6. Rice, J.R., and Rosengren, G.F., *Journal of the Mechanics and Physics of solids*, Vol. 16, 1968, pp. 1-12.
7. Zehnder, A.T., and Rosakis, A.J., *International Journal of Fracture*, Vol. 30, 1986, pp. R43-R48.
8. Marchand, A., Freund, L.B., Ma, C.C., and Duffy, J., "Use of the Shadow Spot Method in Evaluating J for Ductile Steels," Brown University Technical Report, ONR 0597/1, MRL E-160, February 1986.
9. Rosakis, A.J., and Zehnder, A.T., *Journal of Elasticity*, Vol. 15, 1985, pp.347-367.
10. Schreyer, H.L., Kulak, R.F., and Kramer, J.M., *Journal of Pressure Vessel Technology*, Vol. 101, 1979, pp. 226-234.
11. Bathe, K.J., *Finite Element Procedures in Engineering Analysis*, Prentice Hall, 1982.
12. Hinton, E., and Campbell, J.S., *International Journal of Numerical Methods in Engineering*, Vol. 8, 1974, pp. 461-480.
13. Tada, H., Paris, P., and Irwin, G., *The Handbook of Stress Intensity Factors*, Del Research Corporation, 1973.
14. Kumar, V., German, M.D., and Shih, C.F., "An Engineering Approach for Elastic-Plastic Fracture Analysis," EPRI Report NP-1931, July 1981.
15. Rosakis, A.J., and Ravi-Chandar, K., *International Journal of Solids and Structures*, Vol. 22, 1986, pp. 121-134.

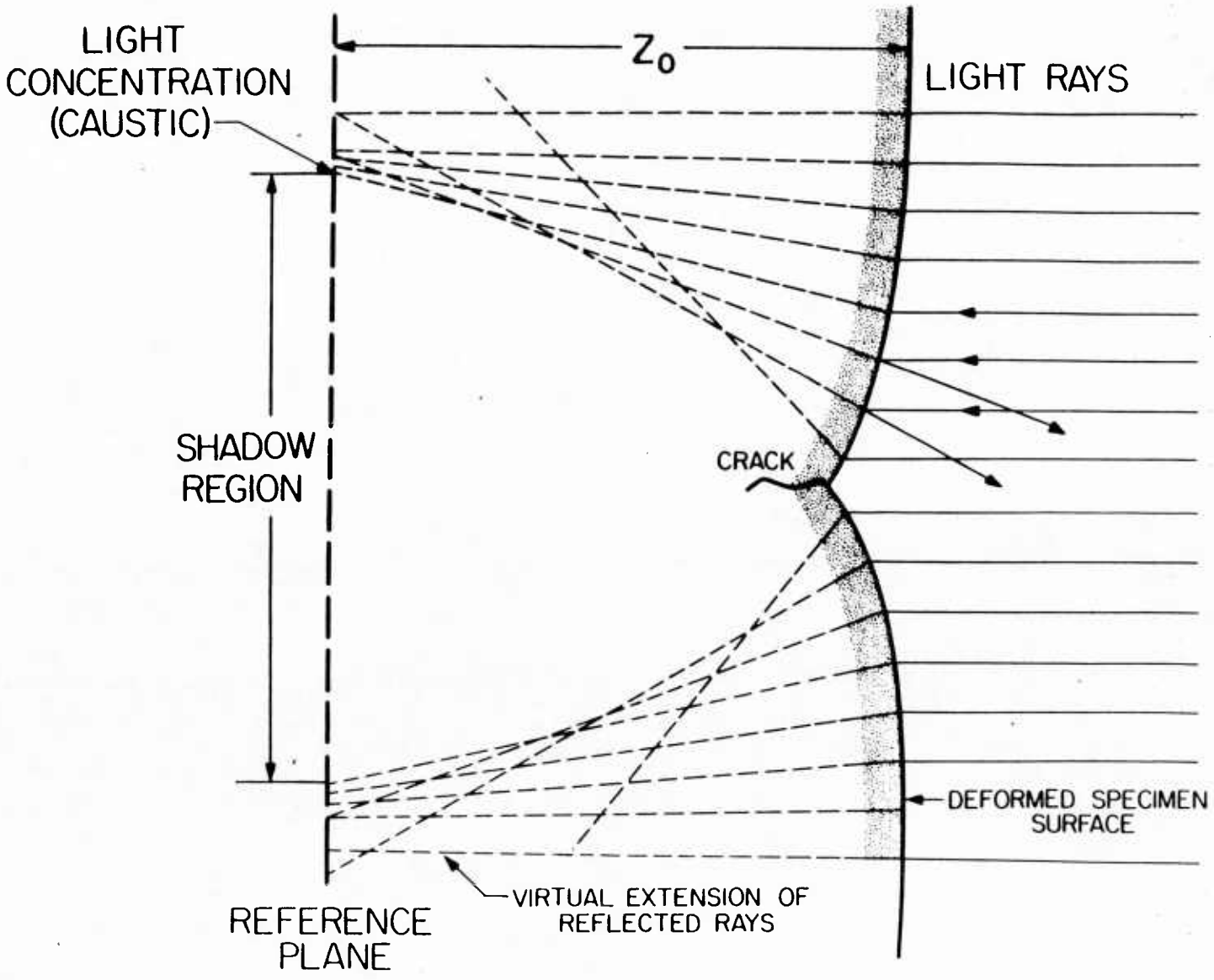

Figure 1. Formation of caustic due to reflection of light from the polished, deformed specimen surface near the crack tip.

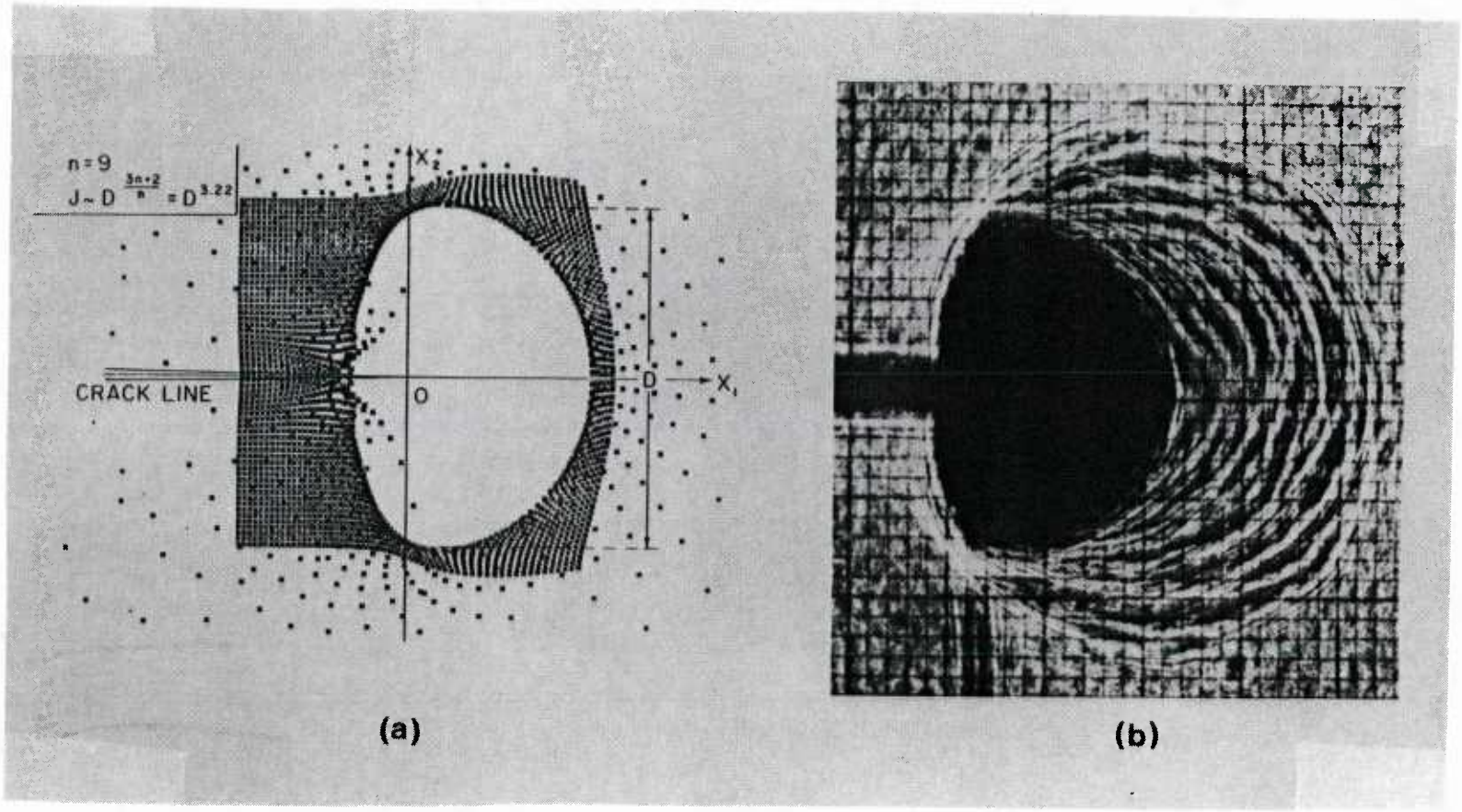

Figure 2. Caustics formed due to reflection of light from within the plane-stress HRR dominant zone. (a) Predicted (from [3]) (b) Experimental.

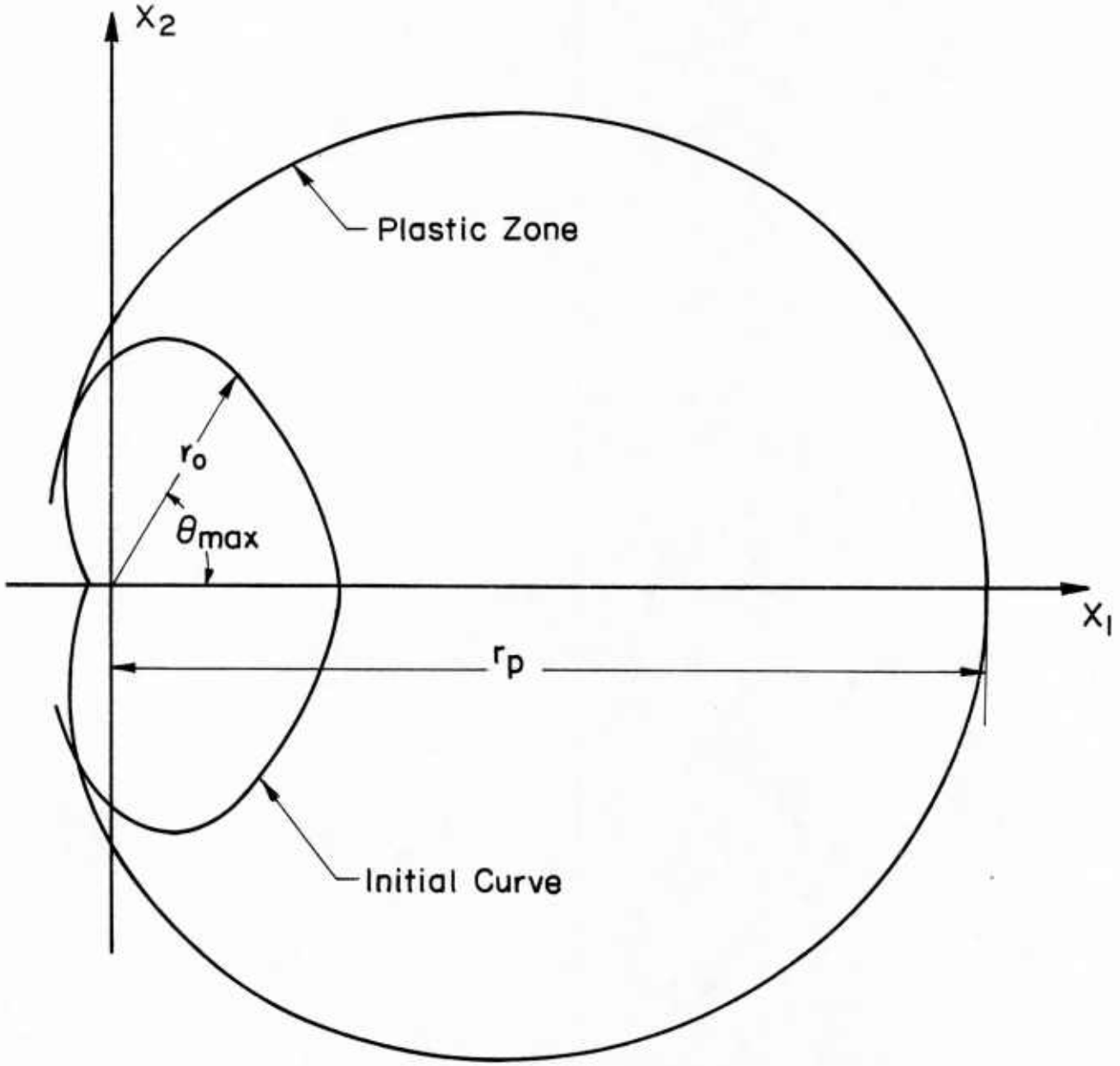

Figure 3. Initial curve and plastic zone geometries.

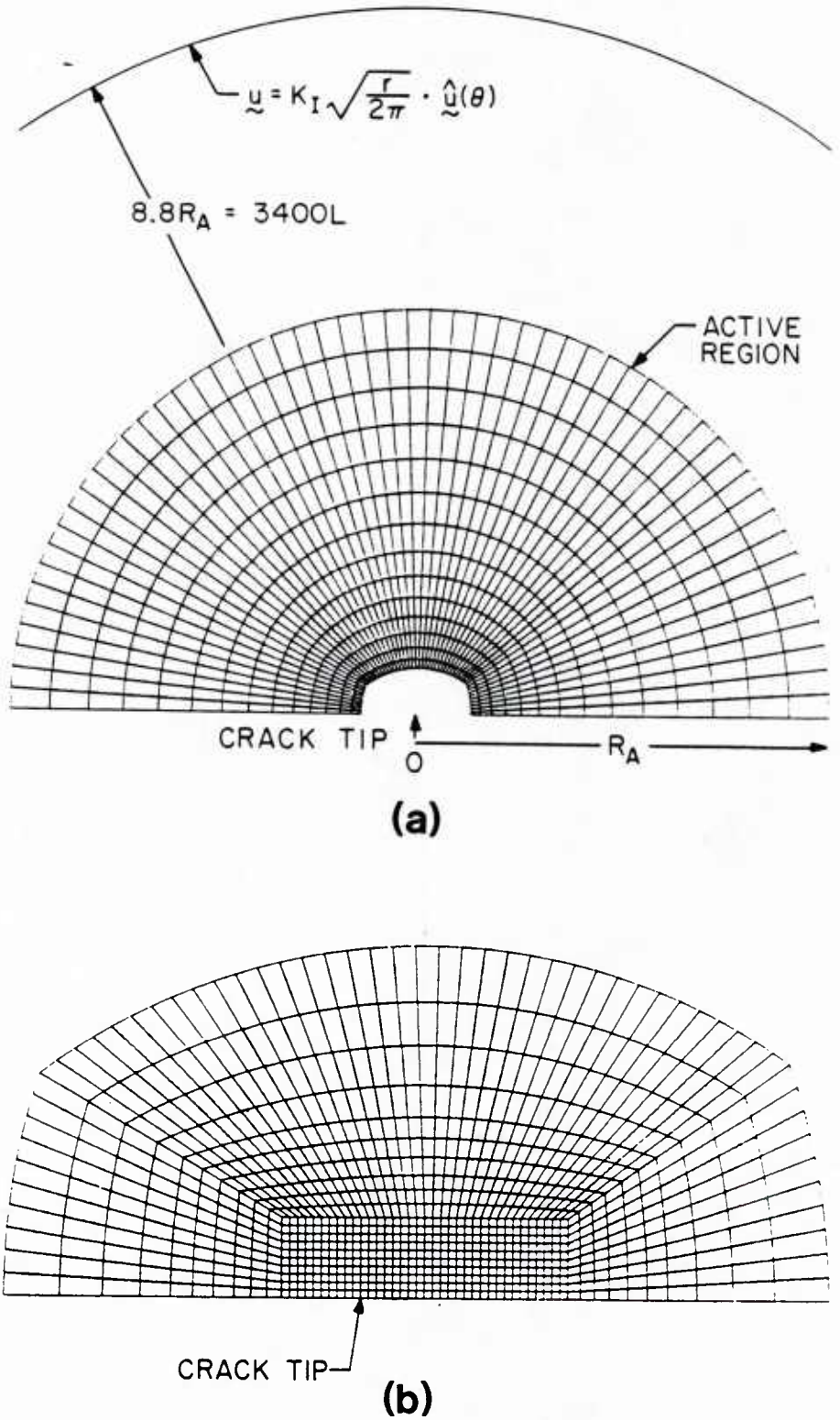

Figure 4. (a) Finite element mesh for numerical model. (b) Detail of mesh near crack tip.

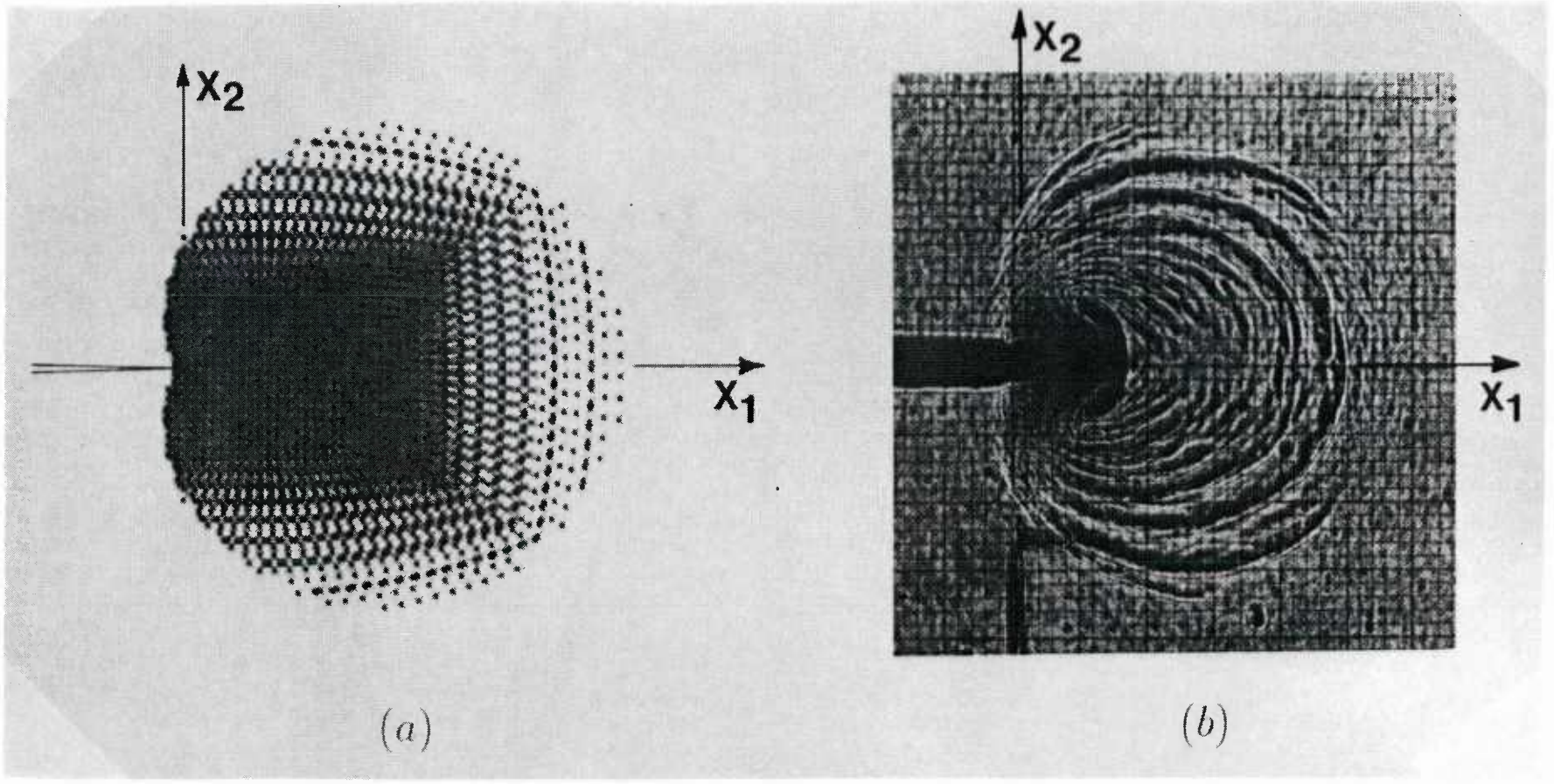

Figure 5. Plane stress plastic zone for n=9. (a) Numerical (b) Experimental.

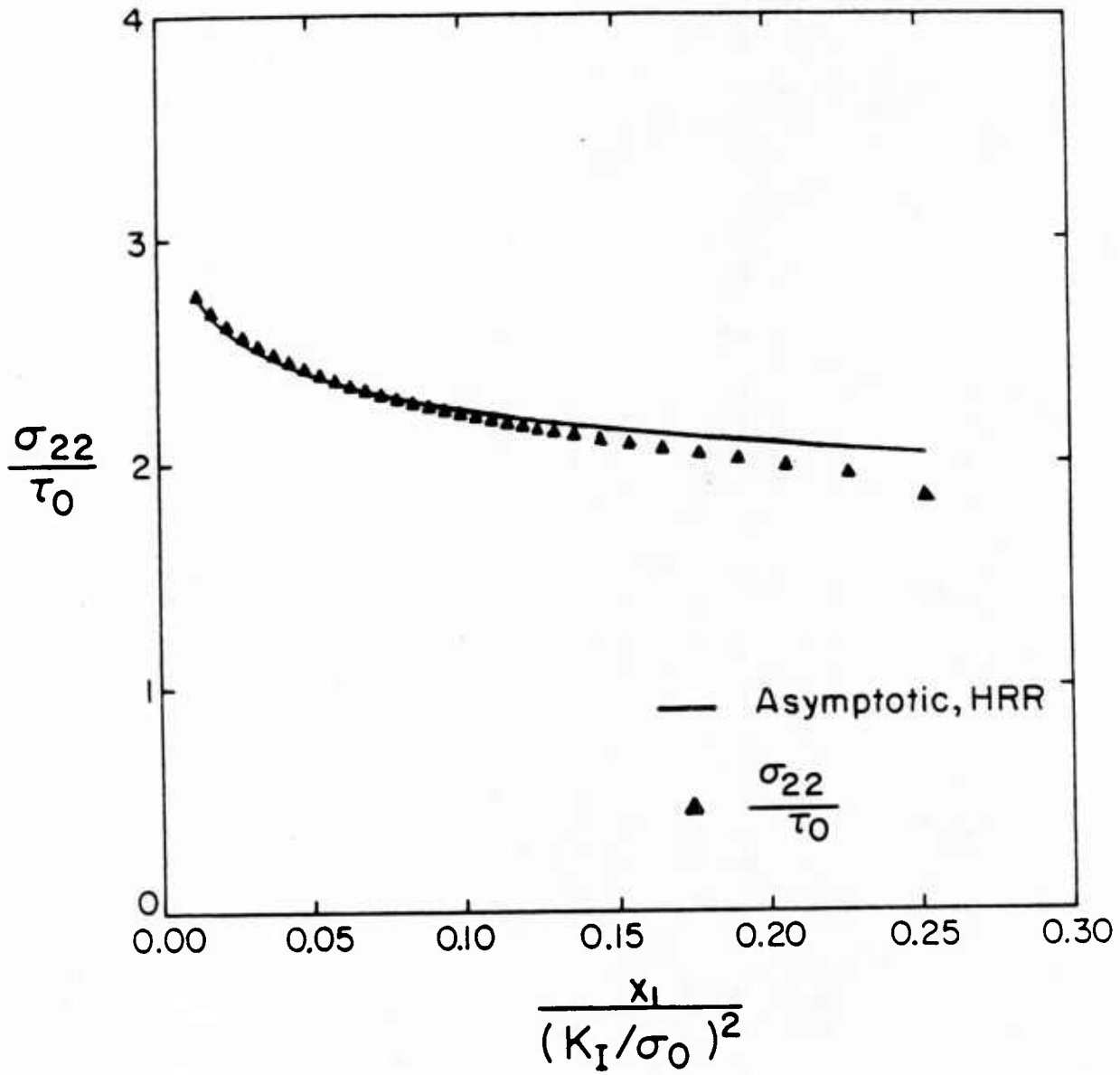

Figure 6. Stress distribution ahead of the crack tip. τ_o = yield stress in shear.

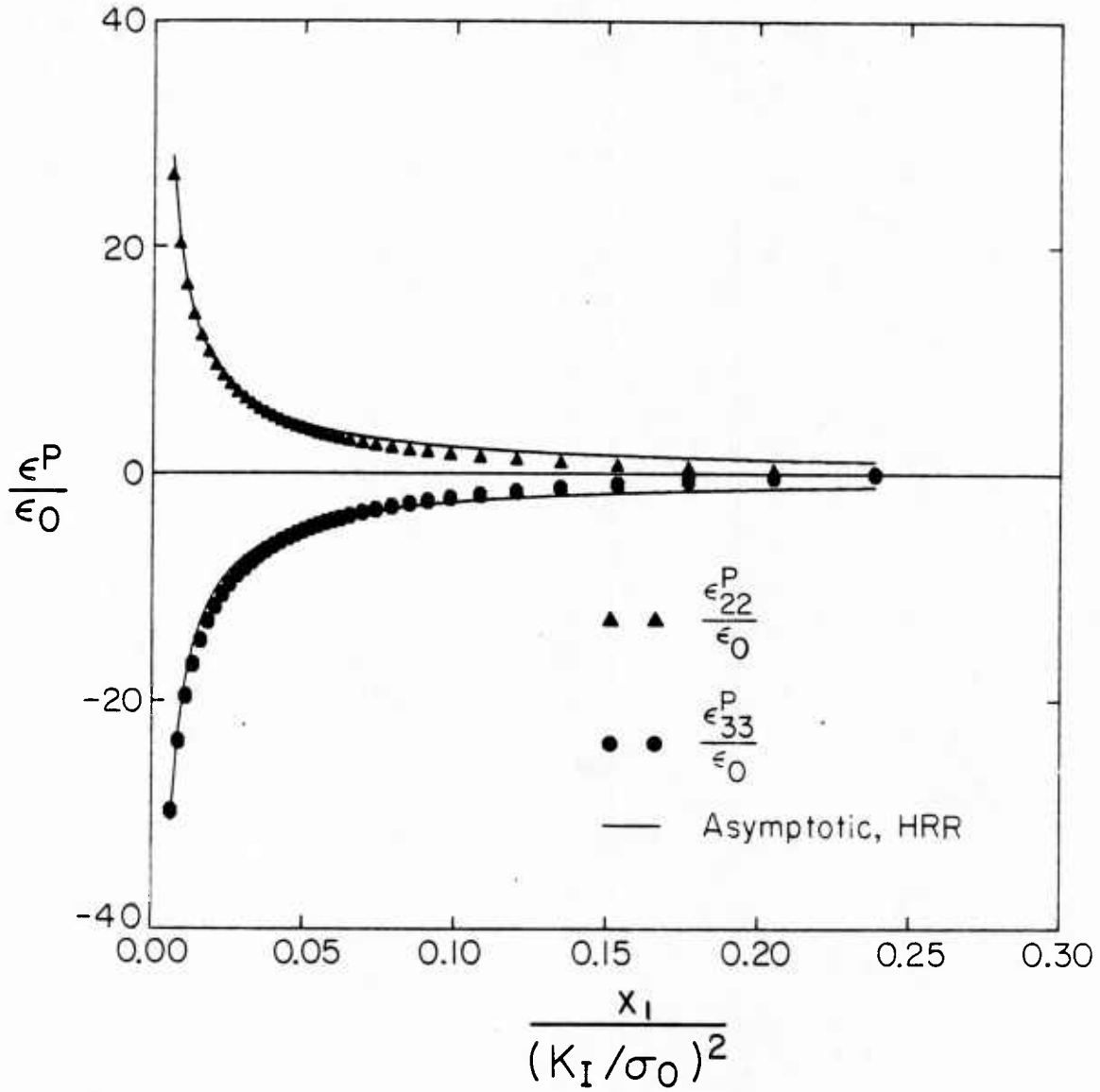

Figure 7. Plastic strain distribution ahead of the crack tip.

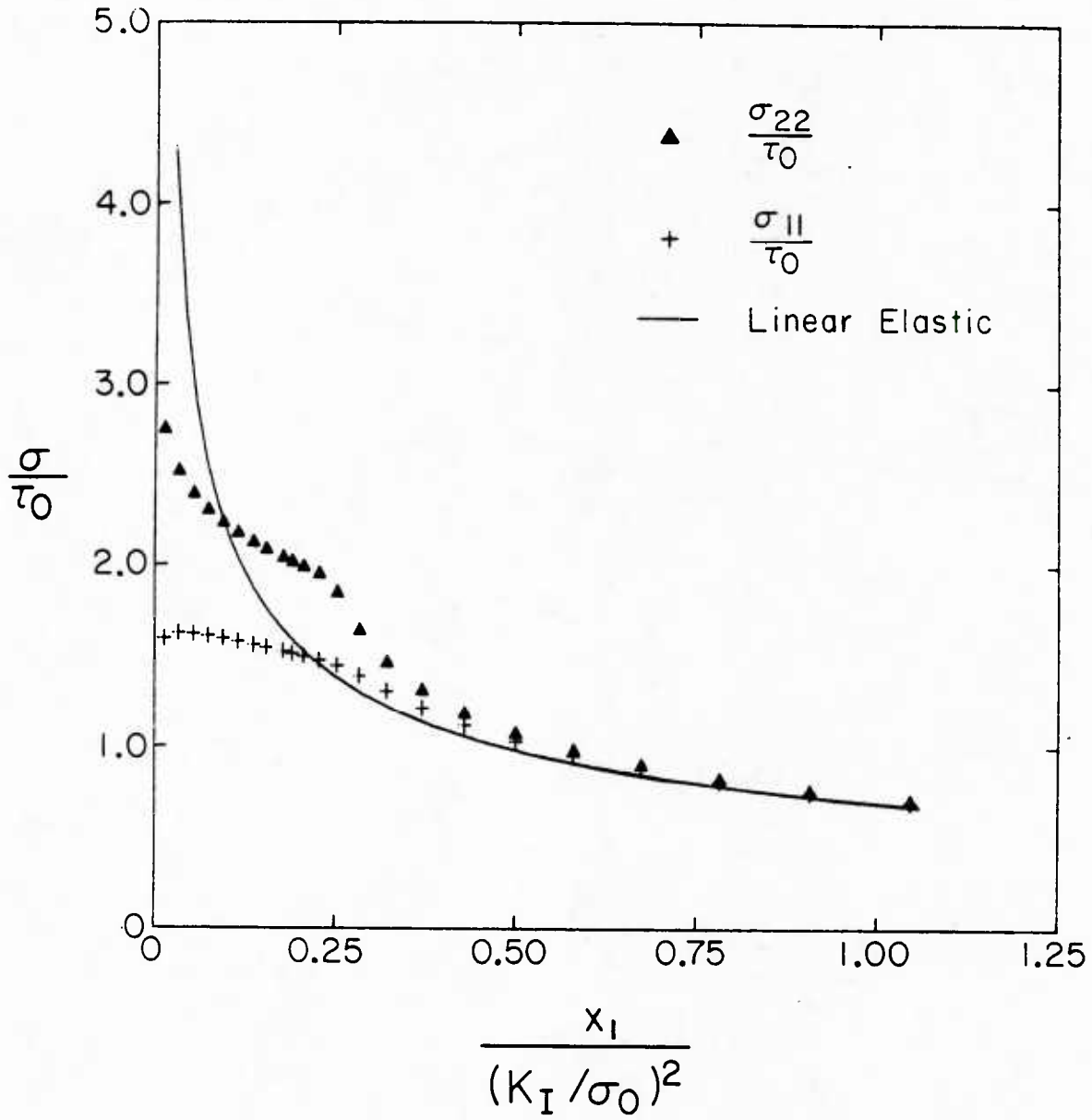

Figure 8. Stress distribution ahead of the crack tip compared to stresses from the linear elastic K_I field.

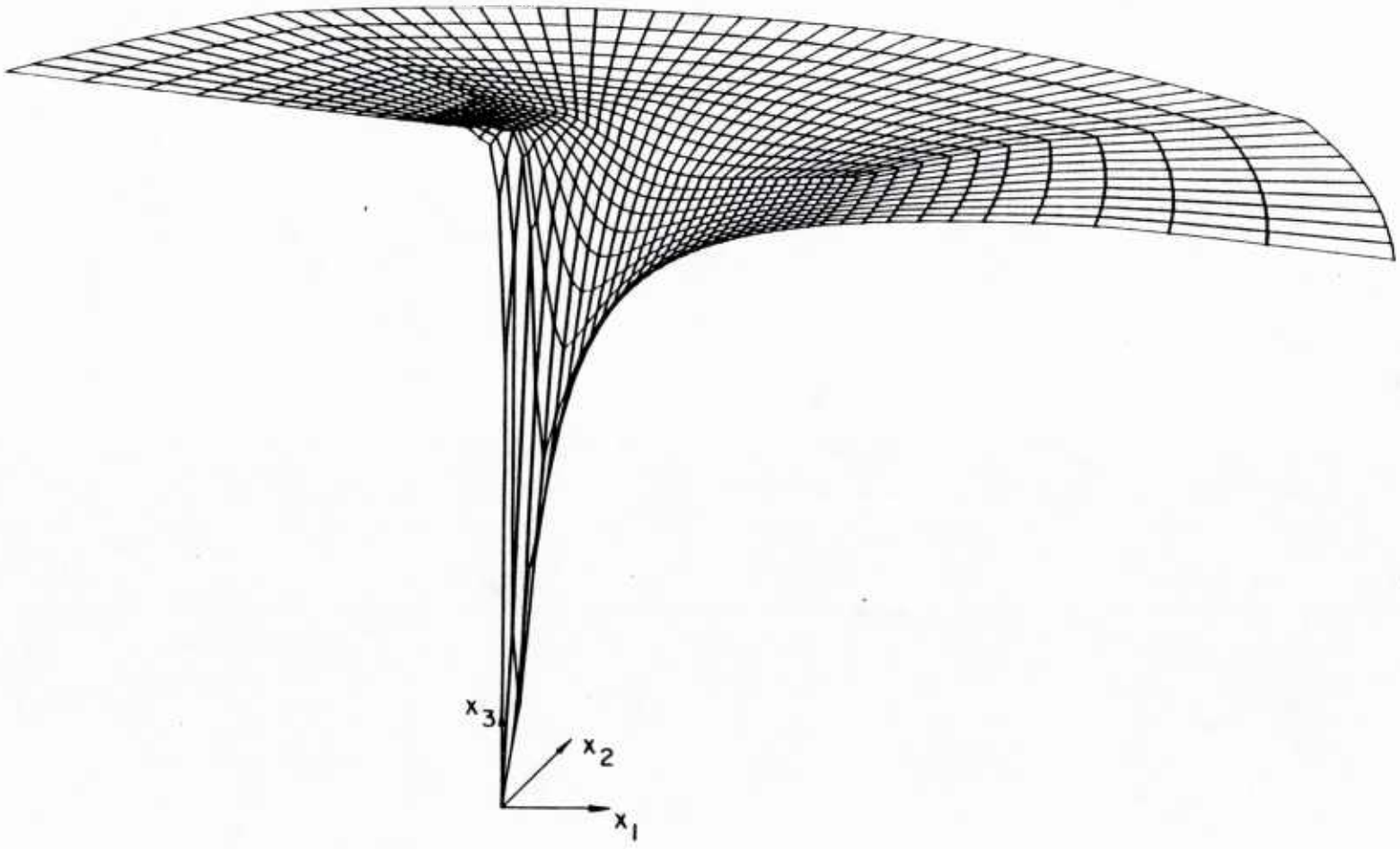

Figure 9. Smoothed out-of-plane displacement field for n=9.

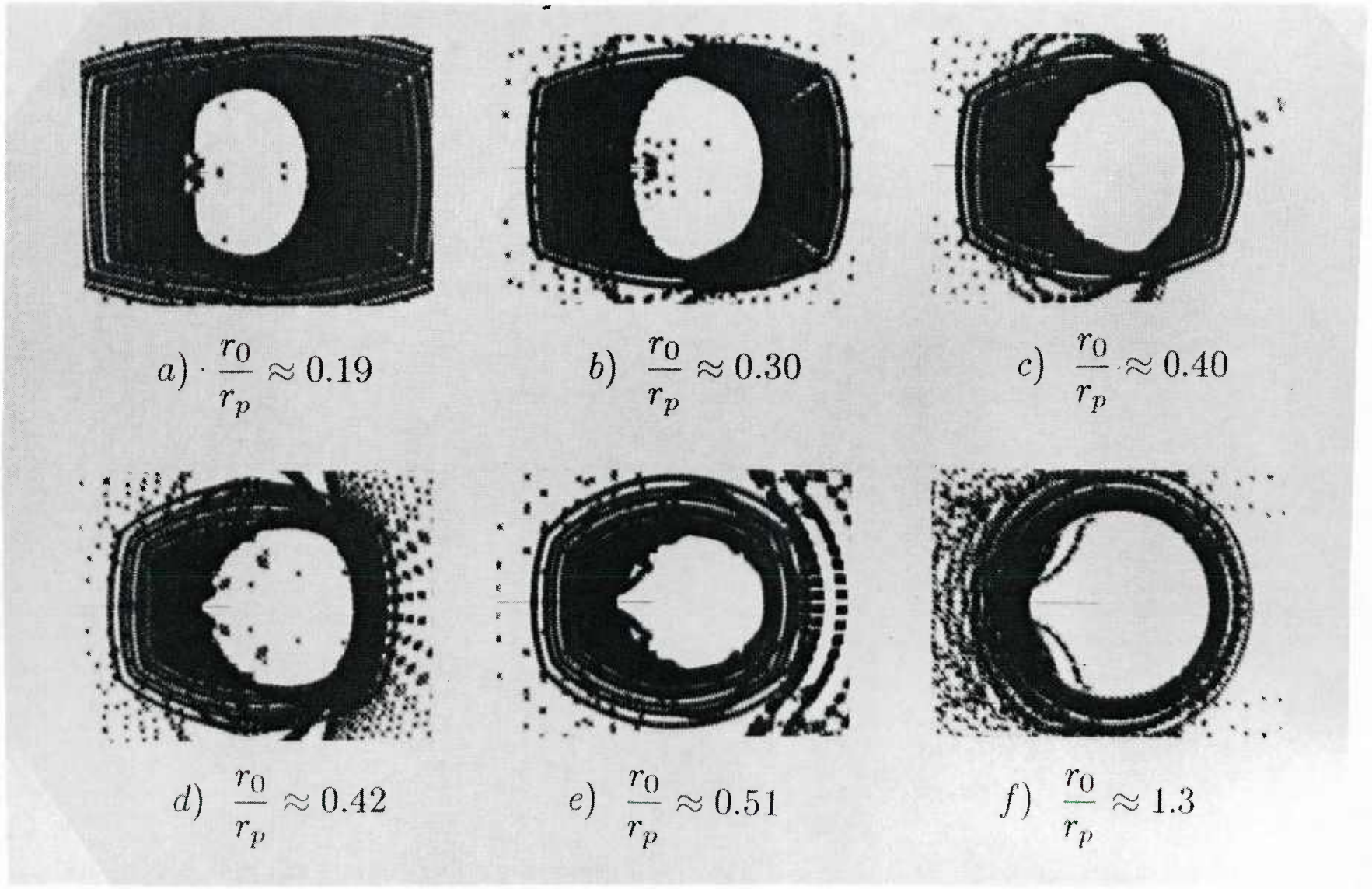

Figure 10. Caustics generated by using the out of plane displacements calculated from the numerical model.

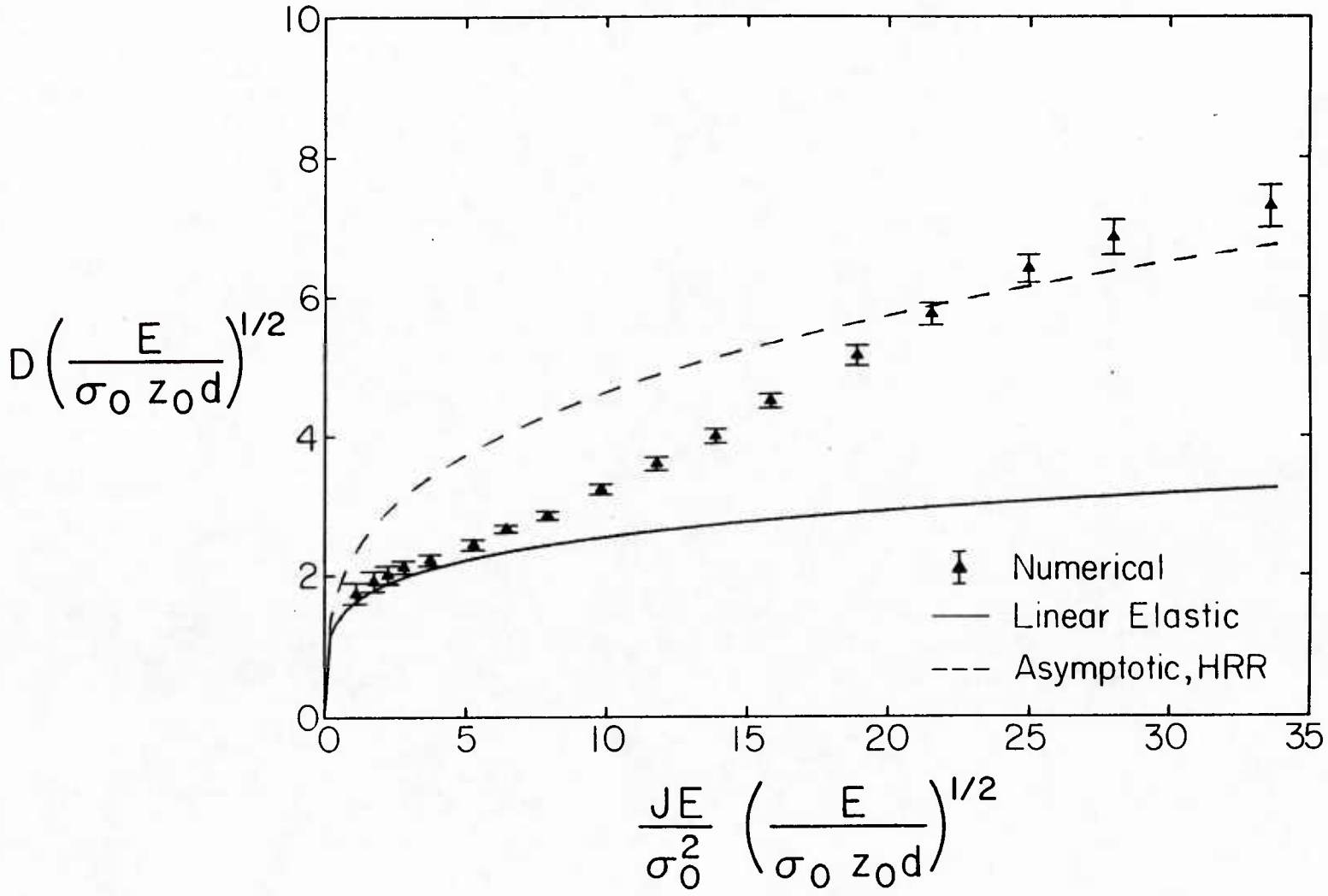

Figure 11. Relation between caustic diameter and J integral.

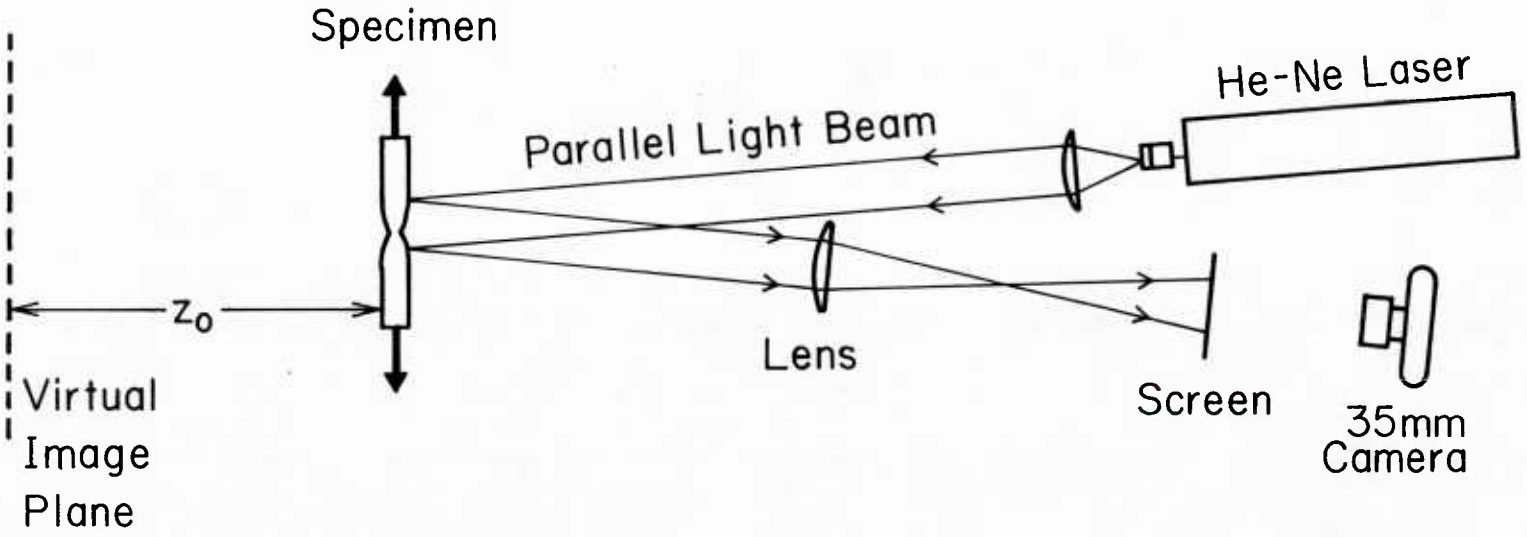

Figure 12. Experimental setup for photographing reflected caustics.

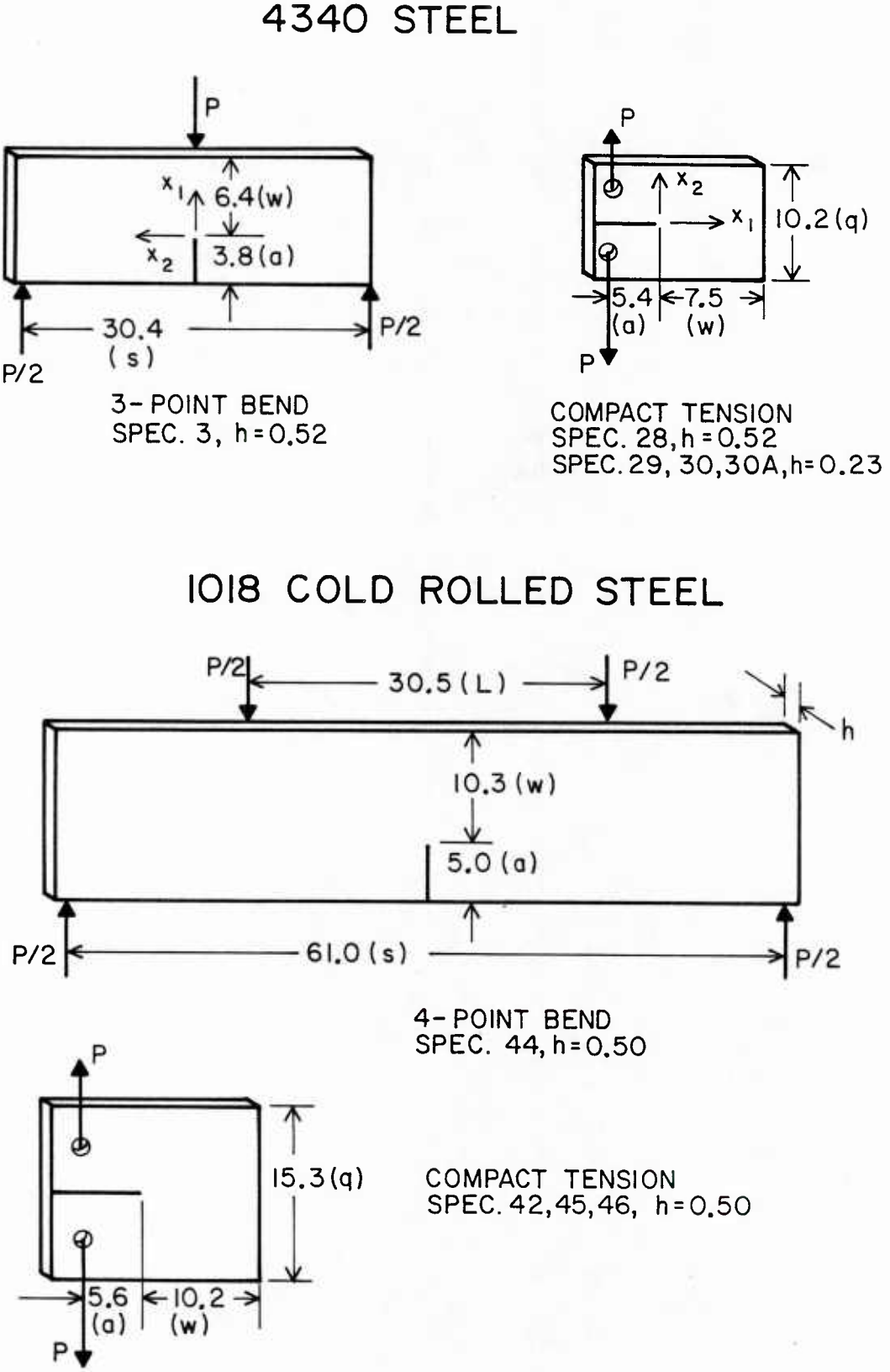

Figure 13. Specimen dimensions and geometries. AH dimensions in cm.

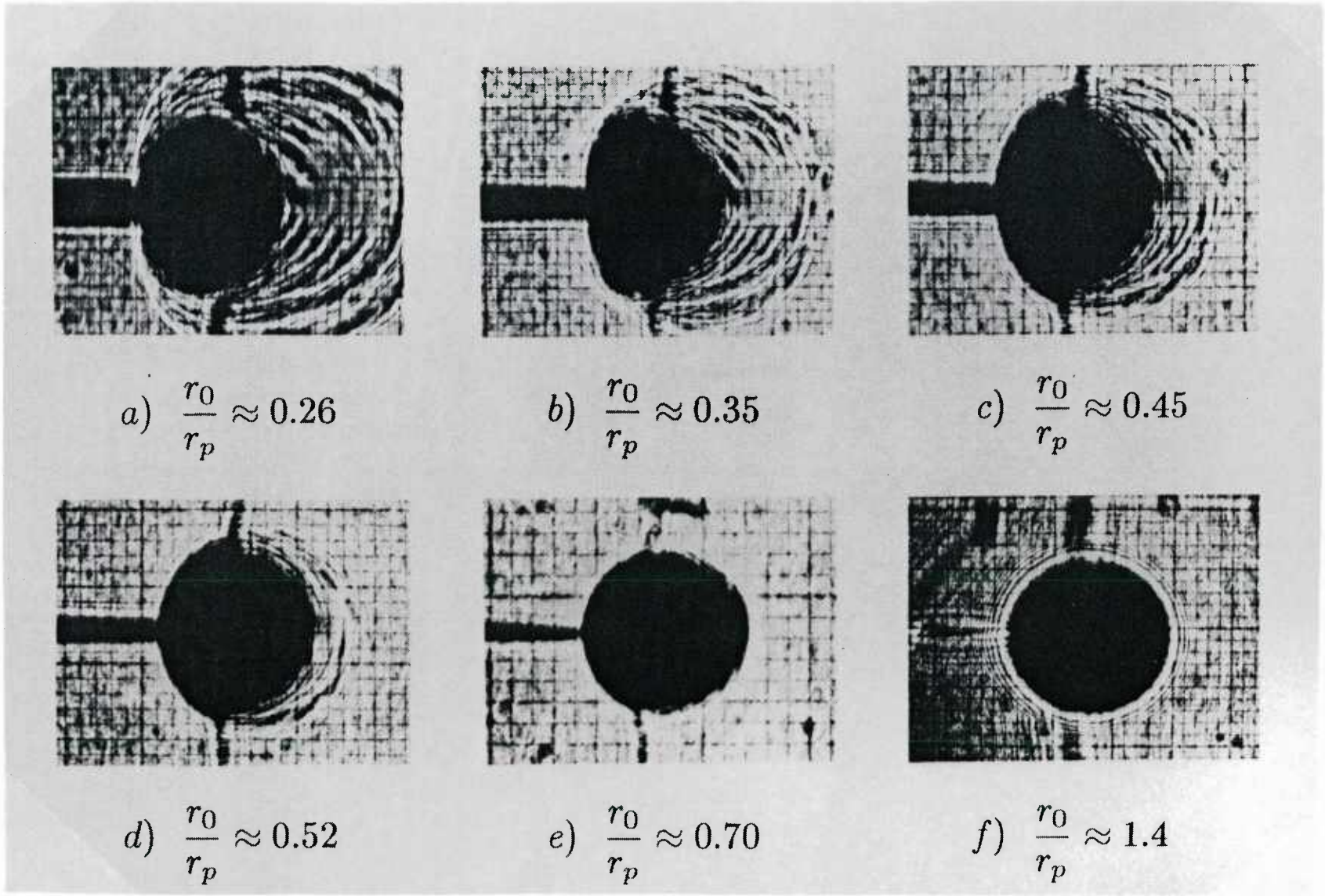

Figure 14. Sequence of caustics obtained for reflection of light from regions near a plastically deforming crack tip.

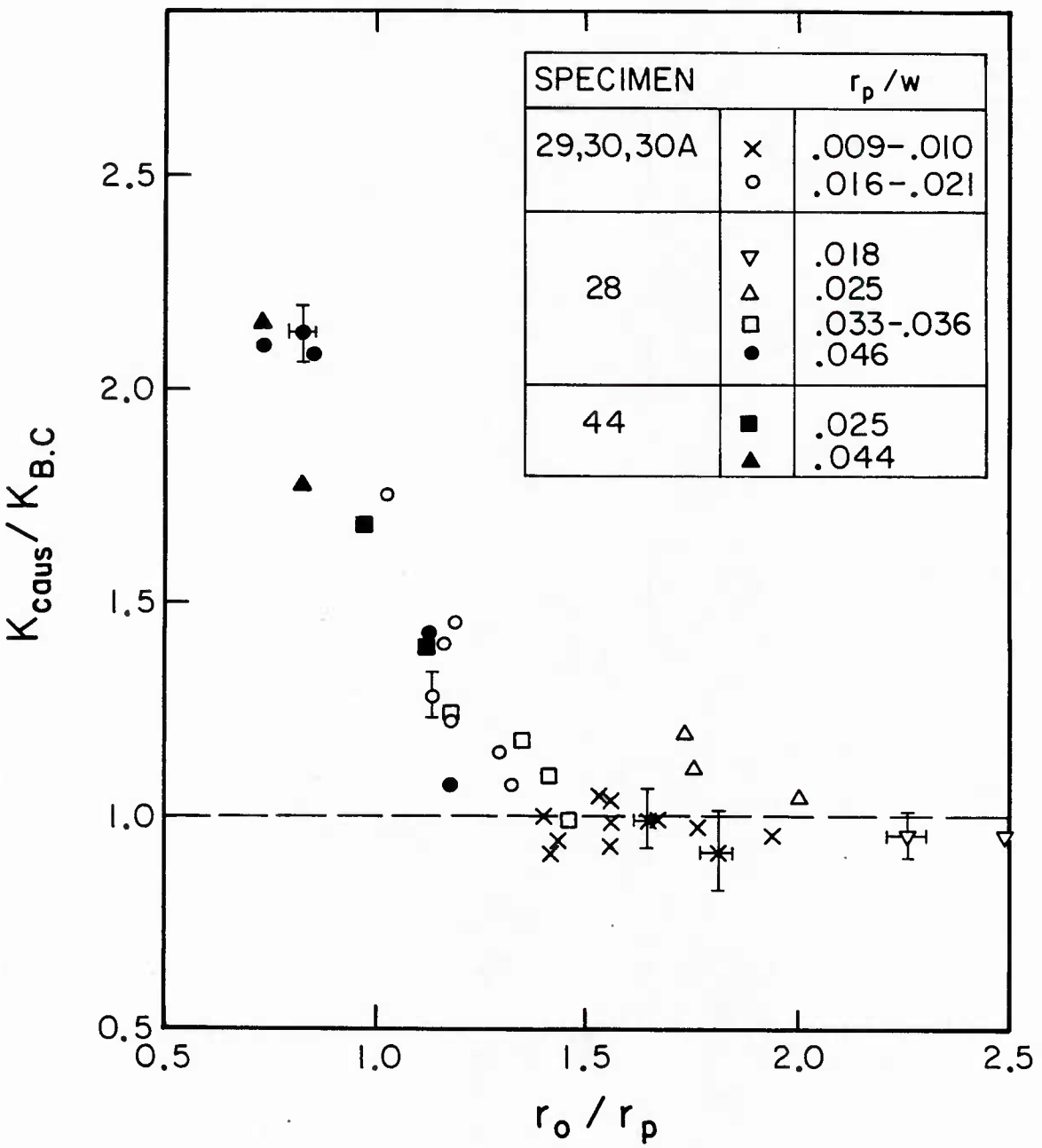

Figure 15. K_{caus}/K_{BC} vs. r_0/r_p. Deviation from 1.0 indicates error caused by plasticity.

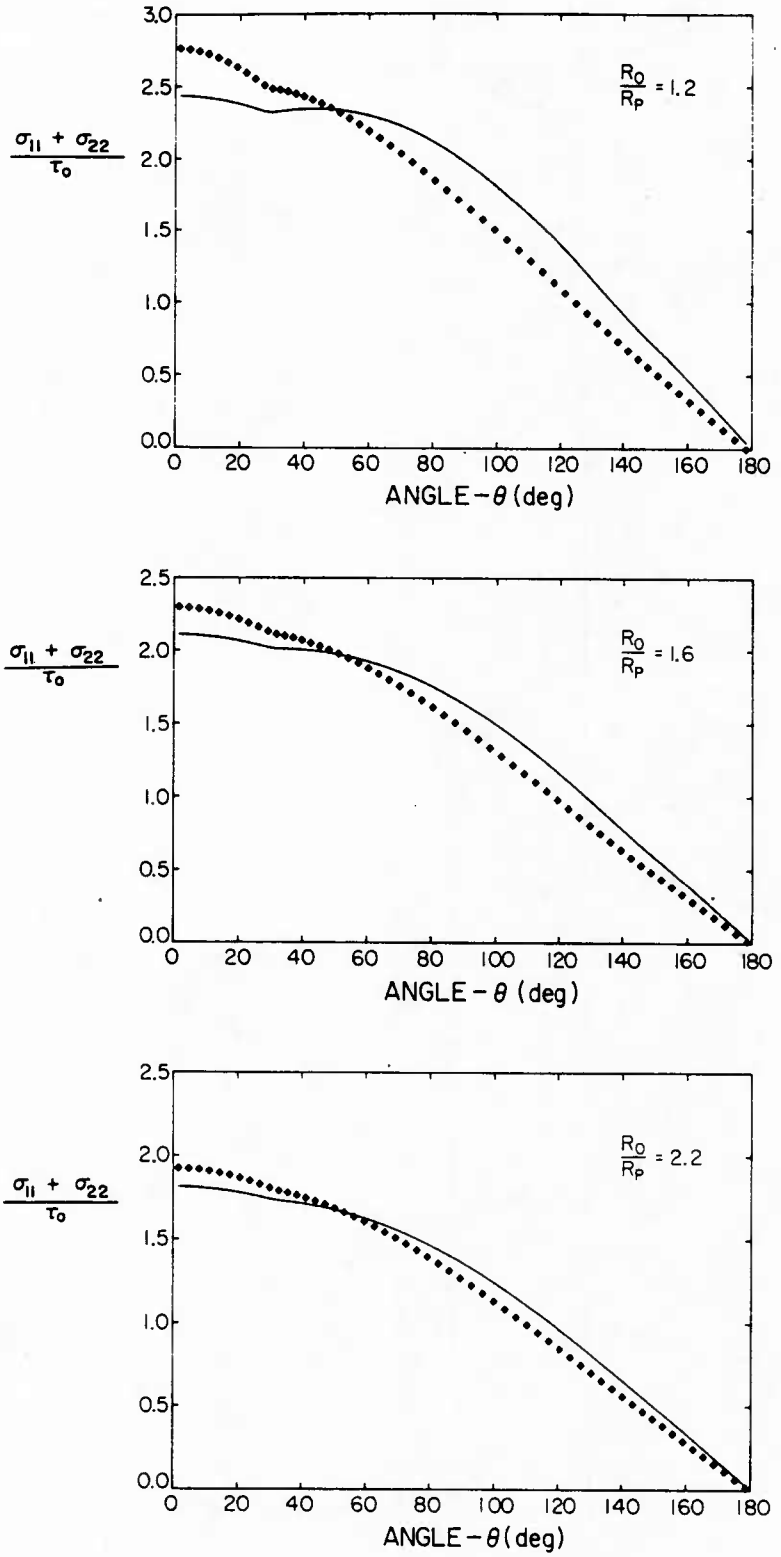

Figure 16. Angular distribution of $(\sigma_{11}+\sigma_{22})$ for different distances from the crack tip. Solid line is stress distribution of K_I field.

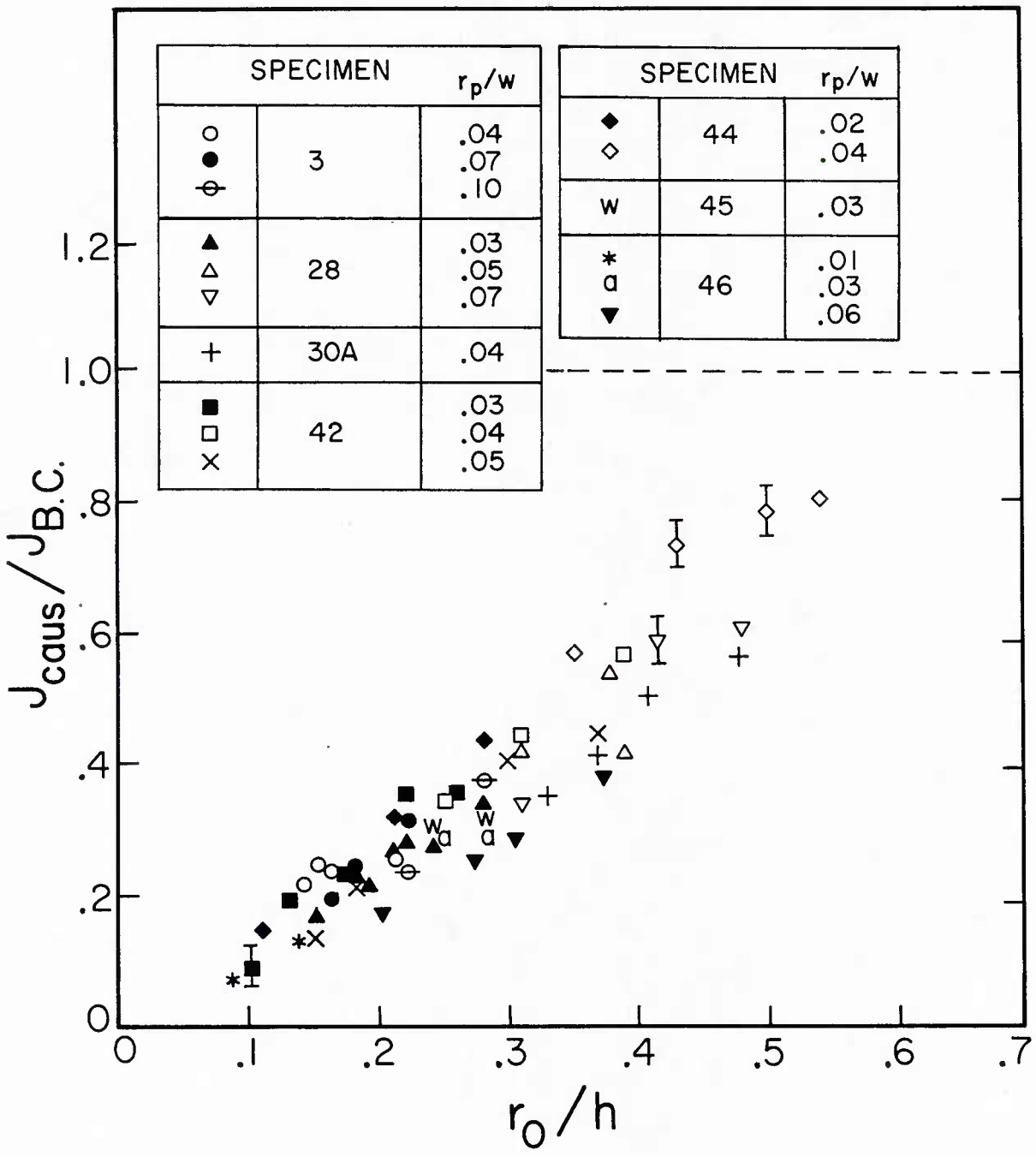

Figure 17. J_{caus}/J_{BC} vs. r_o/h. Deviation from 1.0 indicates error due to three dimensionality for $r_0/h<0.6$.